Exchange-coupled spin-fluctuation theory: calculation of magneto-elastic properties

1997 J. Phys.: Condens. Matter 9 7885

(http://iopscience.iop.org/0953-8984/9/37/019)

J. Phys.: Condens. Matter **9** (1997) 7885–7902. Printed in the UK PII: S0953-8984(97)83066-4

Exchange-coupled spin-fluctuation theory: calculation of magneto-elastic properties

Michael Uhl and Jürgen Kübler

Institut für Festkörperphysik, Technische Hochschule, D-64289 Darmstadt, Germany

Received 2 April 1997, in final form 30 June 1997

Abstract. The local density functional approximation (LDA) is used to calculate magnetic and magneto-elastic properties of itinerant-electron systems at finite temperatures. At the centre of the theory given are spin fluctuations whose modes are coupled by interatomic exchange interactions. The susceptibilities, the Curie temperature, and the thermal expansion coefficients are obtained from a Hamiltonian in which *all* of the parameters are calculated using *ab initio* constrained ground-state total energies. Results are given and compared with experiment for three cases having exceptional magneto-elastic properties; these are γ-Fe, the Invar alloy Fe_3Pt, and γ-Mn.

1. Introduction

Perhaps the best known magneto-elastic effect is that observed in Invar alloys, like e.g. Fe_xNi_{1-x} or Fe_xPt_{1-x}. This effect [1] has now been known of for 100 years, but still attracts a great deal of attention—see for instance the reviews in [2–4].

In attempts to understand this effect theoretically, the early phenomenological two-state model of Weiss [5] and later local density functional calculations [6, 7] suggested that there are two energetically nearly degenerate states: a high-spin state with a large volume and a large magnetic moment, and a low-spin state with a small volume and a small or even vanishing magnetic moment, the energy difference of these being in the thermal range and so permitting longitudinal spin fluctuations that lead to strongly coupled magnetic and elastic degrees of freedom. Subsequently a large number of band-structure calculations were performed for Invar alloys to obtain the total energy, $E(M, V)$, as a function of the magnetic moment M and the volume V [8–13]. By means of a semi-phenomenological Ginzburg–Landau description that goes back to work of Murata and Doniach [14] and others [15–17], the total energy can be used to obtain the phase transition and the temperature dependence of the magnetic properties in weakly magnetic itinerant-electron systems; see e.g. [12, 13, 18–22]. The important point to notice here is that the expansion coefficients of the free energy are extracted from the calculated total energy, whereas the coefficients of the gradient term describing the mode–mode coupling of fluctuations are fitted to experimental results [15, 23].

In a recent publication [24] we showed how *all* of the parameters of the Ginzburg–Landau description can be obtained by means of total-energy calculations. In particular, the gradient term is replaced by a more general coupling term which describes excitation energies that can be obtained from total energies calculated for spin-spiral configurations. Thus magnetic properties such as the Curie temperature and the magnetic susceptibility

0953-8984/97/377885+18$19.50

were calculated *ab initio* for Fe, Co, and Ni, resulting in fair agreement with experimental data [24].

To generalize the theory to describe magneto-elastic properties, we must include fluctuations of the volume in addition to those of the magnetization. Furthermore, in contrast to the case for the transition metals, Fe, Co, and Ni, where the total energy as a function of the magnetic moment can be approximated well using a rather small number of expansion coefficients [24], the magnetic ordering in γ-Fe and the Invar alloy Fe_3Pt depends sensitively on the magnitude of the magnetic moment or the volume, as has been shown in earlier work [25, 26]. Here, in Taylor series expansions of the total energy, we must take into account a large number of terms involving powers of the magnetization M and the volume V. Thus, applying the theory to γ-Fe and Fe_3Pt, we plot the total-energy curves of the collinear and non-collinear spin arrangements, and use them to extract the parameters valid for the spin-fluctuation Hamiltonian of each particular system. Using this Hamiltonian in a mean-field theory, the temperature dependence of the magneto-elastic properties is obtained, and the Curie temperature as well as the thermal expansion coefficient are calculated and compared with experimental results. Finally, we focus our attention on γ-Mn for which the antiferromagnetic ordering not only is connected with a volume expansion but also is accompanied by a tetragonal lattice distortion which decreases with decreasing order parameter and vanishes above the Néel temperature. We present *ab initio* calculations for the Néel temperature and show the distortion parameter as a function of the temperature.

2. Spin-fluctuation theory

2.1. The total energy

To describe magneto-elastic properties of metallic systems, we assume that the Hamiltonian $\mathcal{H}$ is a functional of the magnetization $\boldsymbol{M}(\boldsymbol{r})$ and the volume $V(\boldsymbol{r})$, i.e. $\mathcal{H}[\boldsymbol{M}(\boldsymbol{r}), V(\boldsymbol{r})]$ at any point $\boldsymbol{r}$ in space. Thus, the total energy at $T = 0$ K is a function of the ground-state values $\tilde{\boldsymbol{M}}$ and V: $E(\tilde{\boldsymbol{M}}, V)$. Simplifying here, we restrict the $\boldsymbol{r}$-dependence of the Hamiltonian to values of $\boldsymbol{r}$ on the crystal lattice which we denote by $\{\boldsymbol{R}\}$. We thus omit any fluctuations of the magnetization on a scale smaller than the interatomic distances. This is an atomic sphere approximation because the magnetization vector of an atom at site $\boldsymbol{R}$ is characteristic for the entire atom at this site and the interstitial plays no role.

The magnetization $\tilde{\boldsymbol{M}}$ of the ground state is not necessarily ferromagnetic, but may be defined by the magnitude of the magnetization M, a wave vector $\boldsymbol{q}$ describing the propagation vector of a spiral, and a polar angle θ, such that the magnetic moment of an atom at the site $\boldsymbol{R}$ in the crystal is given in Cartesian coordinates by

$$\tilde{\boldsymbol{M}} = M(\cos(\boldsymbol{q}\cdot\boldsymbol{R})\sin\theta, \sin(\boldsymbol{q}\cdot\boldsymbol{R})\sin\theta, \cos\theta). \tag{1}$$

For instance, a ferromagnet might be specified by the polar angle $\theta = 0^\circ$:

$$\tilde{\boldsymbol{M}} = M(0, 0, 1) \tag{2}$$

and an antiferromagnetic spiral configuration having a vanishing net magnetization by $\theta = 90^\circ$:

$$\tilde{\boldsymbol{M}} = M(\cos(\boldsymbol{q}\cdot\boldsymbol{R}), \sin(\boldsymbol{q}\cdot\boldsymbol{R}), 0) \tag{3}$$

which in particular defines a collinear antiferromagnet if $2\boldsymbol{q}$ is a reciprocal-lattice vector, since in this case $\cos(\boldsymbol{q}\cdot\boldsymbol{R}) = \pm 1$ and $\sin(\boldsymbol{q}\cdot\boldsymbol{R}) = 0$.

We obtain the total energy $E(\tilde{\boldsymbol{M}}, V)$ numerically by means of constrained non-collinear band-structure calculations using the non-collinear fixed-spin-moment method described in

[25, 26]. In [26] it was also shown that the total energy can be separated with good accuracy into a volume-dependent contribution E_C of the collinear configuration and a volume-independent non-collinear contribution E_Q, which describes the energy difference between spin configurations of different wave vectors $\boldsymbol{q}$: $E(\tilde{\boldsymbol{M}}, V) \simeq E_C(M, V) + E_Q(M, \boldsymbol{q}, \theta)$. This suggests that, for an analytic treatment, we may expand the energy contributions E_C and E_Q in powers of V and M, where, because of time-reversal symmetry, only even powers of M occur. Furthermore, since numerical calculations show that $E_Q(M, \boldsymbol{q}, \theta) \propto \sin^2\theta$, we may thus write the total energy $E(\tilde{\boldsymbol{M}}, V)$ as

$$E(\tilde{\boldsymbol{M}}, V) = \sum_{n=0}^{n_{\max}} \sum_{m=0}^{m_{\max}} A_{nm} M^{2n} V^m + \sin^2\theta \sum_{n=1}^{n_{\max}} J_n(\boldsymbol{q}) M^{2n}. \tag{4}$$

This expansion defines the quantities A_{nm} and $J_n(\boldsymbol{q})$ which may thus be calculated from total-energy differences. It was used by us previously in [24], where, however, we did not consider any volume dependence. The appropriate values of $n_{\max}$ and $m_{\max}$ will be specified in section 3.

2.2. The Hamiltonian

The Hamiltonian of the crystal possessing magnetic moments $\boldsymbol{M}(\boldsymbol{R})$ and volume $V(\boldsymbol{R})$ is now written as

$$\mathcal{H} = \frac{1}{N} \sum_{\boldsymbol{R}} \Phi_C(\boldsymbol{M}(\boldsymbol{R}), V(\boldsymbol{R})) + \frac{1}{N} \sum_{\boldsymbol{R}} \sum_{\boldsymbol{R}'} \Phi_Q(\boldsymbol{M}(\boldsymbol{R}), \boldsymbol{M}(\boldsymbol{R}')). \tag{5}$$

For this Hamiltonian to yield the total energy given by (4), the first term on the right-hand side, Φ_C, denotes the collinear part of the total energy and is given by an expansion in powers of $\boldsymbol{M}^2(\boldsymbol{R})$ and $V(\boldsymbol{R})$ as

$$\Phi_C(\boldsymbol{M}(\boldsymbol{R}), V(\boldsymbol{R})) = \sum_{n,m} A_{nm} \boldsymbol{M}^{2n}(\boldsymbol{R}) V^m(\boldsymbol{R}). \tag{6}$$

The second term on the right-hand side, Φ_Q, originates from the non-collinear part of the total energy and contains a description of magnetic exchange between the magnetic moments on different sites, $\boldsymbol{M}(\boldsymbol{R})$ and $\boldsymbol{M}(\boldsymbol{R}')$. It is written as a Taylor series expansion as

$$\Phi_Q(\boldsymbol{M}(\boldsymbol{R}), \boldsymbol{M}(\boldsymbol{R}')) = \sum_n J_n(\boldsymbol{R} - \boldsymbol{R}') \boldsymbol{M}^{2n}(\boldsymbol{R})(\boldsymbol{M}(\boldsymbol{R}) \cdot \boldsymbol{M}(\boldsymbol{R}')). \tag{7}$$

Here the $J_n(\boldsymbol{R} - \boldsymbol{R}')$ denote exchange constants for different sites, $\boldsymbol{R}$ and $\boldsymbol{R}'$, which are connected with the quantity $J_n(\boldsymbol{q})$ defined in (4) by the lattice Fourier transform

$$J_n(\boldsymbol{R} - \boldsymbol{R}') = \frac{1}{N} \sum_{\boldsymbol{k}} J_n(\boldsymbol{k}) \exp(\mathrm{i}\boldsymbol{k} \cdot (\boldsymbol{R} - \boldsymbol{R}')). \tag{8}$$

To treat fluctuations at finite temperatures, the classical fields, $\boldsymbol{M}(\boldsymbol{R})$ and $V(\boldsymbol{R})$, are decomposed into average values, $\tilde{\boldsymbol{M}}$ and V, and fluctuations of the magnetization $m_j(\boldsymbol{R})$ (where $j = X, Y, Z$ denotes Cartesian components) and the volume $w(\boldsymbol{R})$:

$$\boldsymbol{M}(\boldsymbol{R}) = \tilde{\boldsymbol{M}} + \sum_j m_j(\boldsymbol{R}) \boldsymbol{e}_j \tag{9}$$

$$V(\boldsymbol{R}) = V + w(\boldsymbol{R}). \tag{10}$$

Because of the periodicity of the crystal, the fluctuations $m_j(\boldsymbol{r})$ and $w(\boldsymbol{r})$ are given by lattice Fourier transforms:

$$m_j(\boldsymbol{R}) = \sum_{\boldsymbol{k}\in 1BZ} m_{j\boldsymbol{k}} \exp(\mathrm{i}\boldsymbol{k}\cdot\boldsymbol{R}) \tag{11}$$

$$w(\boldsymbol{R}) = \sum_{\boldsymbol{k}\in 1BZ} w_{\boldsymbol{k}} \exp(\mathrm{i}\boldsymbol{k}\cdot\boldsymbol{R}) \tag{12}$$

where the wave vector $\boldsymbol{k}$ lies in the first Brillouin zone (1BZ).

2.3. The free energy

Using the abbreviation $\beta = (k_B T)^{-1}$, we write the partition function $\mathcal{Z}$ and the free energy $\mathcal{F}$ as $\mathcal{Z} = \int \mathrm{d}\Gamma \exp(-\beta\mathcal{H})$ and $\mathcal{F} = -\beta^{-1}\ln\mathcal{Z}$. Here $\int \mathrm{d}\Gamma$ denotes the classical integral over the phase space of fluctuations. Because the fluctuations $m_j(\boldsymbol{R})$ and $w(\boldsymbol{R})$ are real, the number of independent variables is restricted by $m_{j,+\boldsymbol{k}} = m^*_{j,-\boldsymbol{k}} = x_{j\boldsymbol{k}} + \mathrm{i}y_{j\boldsymbol{k}}$ and $w_{+\boldsymbol{k}} = w^*_{-\boldsymbol{k}} = x_{0\boldsymbol{k}} + \mathrm{i}y_{0\boldsymbol{k}}$. Thus the integral over phase space is given by

$$\int \mathrm{d}\Gamma = \Big(\prod_{j\boldsymbol{k}}{}' \int \mathrm{d}x_{j\boldsymbol{k}} \int \mathrm{d}y_{j\boldsymbol{k}}\Big)\Big(\prod_{\boldsymbol{k}}{}' \int \mathrm{d}x_{0\boldsymbol{k}} \int \mathrm{d}y_{0\boldsymbol{k}}\Big) \tag{13}$$

where the prime denotes that the product includes only one $\boldsymbol{k}$-vector of the pair $(+\boldsymbol{k}, -\boldsymbol{k})$.

With the Hamiltonian given by (5), the partition function $\mathcal{Z}$ cannot be evaluated exactly. Therefore, the free energy $\mathcal{F}$ is approximated by the Peierls–Feynman inequality:

$$\mathcal{F} \leqslant \mathcal{F}_{SF} = \mathcal{F}_0 + \langle\mathcal{H}\rangle_0 - \langle\mathcal{H}_0\rangle_0. \tag{14}$$

For the so-called model Hamiltonian, $\mathcal{H}_0$, we use the quadratic form

$$\mathcal{H}_0 = \sum_{j\boldsymbol{k}} a_{j\boldsymbol{k}}|m_{j\boldsymbol{k}}|^2 + \sum_{\boldsymbol{k}} b_{\boldsymbol{k}}|w_{\boldsymbol{k}}|^2 \tag{15}$$

thus reducing the functional integration to Gaussian integrals. The free energy corresponding to $\mathcal{H}_0$ is given by $\mathcal{F}_0 = -\beta^{-1}\ln\mathcal{Z}_0$ where $\mathcal{Z}_0 = \int \mathrm{d}\Gamma \exp(-\beta\mathcal{H}_0)$ and $\langle\ \rangle_0$ denotes a thermal average calculated with the model partition function $\mathcal{Z}_0$. The approximate free energy $\mathcal{F}_{SF}$ is thus calculated to be

$$\mathcal{F}_{SF} = -\frac{1}{2\beta}\sum_{j\boldsymbol{k}} \ln\left(\frac{\pi}{2\beta a_{j\boldsymbol{k}}}\right) - \frac{1}{2\beta}\sum_{\boldsymbol{k}} \ln\left(\frac{\pi}{2\beta b_{\boldsymbol{k}}}\right) + \langle\mathcal{H}\rangle_0 - \langle\mathcal{H}_0\rangle_0. \tag{16}$$

Finally, the coefficients $a_{j\boldsymbol{k}}$ and $b_{\boldsymbol{k}}$ appearing here are obtained variationally, i.e. they are chosen as those which minimize the free energy: $\partial\mathcal{F}_{SF}/\partial a_{j\boldsymbol{k}} = 0$ and $\partial\mathcal{F}_{SF}/\partial b_{\boldsymbol{k}} = 0$. To carry out this calculation we next express the thermal averages $\langle\mathcal{H}\rangle_0$ and $\langle\mathcal{H}_0\rangle_0$ in terms of $a_{j\boldsymbol{k}}$ and $b_{\boldsymbol{k}}$.

2.4. Calculation of thermal averages

In general, the thermal average of a function, F, that depends on the fluctuations $x_{j\boldsymbol{k}}$ is determined by

$$\langle F(x_{j\boldsymbol{k}})\rangle_0 = \Big(\int \mathrm{d}\Gamma\ F(x_{j\boldsymbol{k}}) \exp(-\beta\mathcal{H}_0)\Big)\Big/\Big(\int \mathrm{d}\Gamma\ \exp(-\beta\mathcal{H}_0)\Big). \tag{17}$$

Because of the simple model Hamiltonian $\mathcal{H}_0$, the averages are Gaussian integrals, and one obtains easily for even powers of $x_{j\boldsymbol{k}}$ and $y_{j\boldsymbol{k}}$

$$\langle x^{2n}_{j\boldsymbol{k}}\rangle_0 = (2n-1)!!(4\beta a_{j\boldsymbol{k}})^{-n} = (2n-1)!!\langle x^2_{j\boldsymbol{k}}\rangle^n_0 \tag{18}$$

whereas averages of odd powers vanish, $\langle x_{jk}^{2n-1}\rangle_0 = 0$. (For $j = 0$ the quantity a_{jk} stands for b_k.) Thus, in the following we may replace the coefficients a_{jk} and b_k by the average values $\langle|m_{jk}|^2\rangle_0 = \langle x_{jk}^2\rangle_0 + \langle y_{jk}^2\rangle_0$ and $\langle|w_k|^2\rangle_0 = \langle x_{0k}^2\rangle_0 + \langle y_{0k}^2\rangle_0$ in the form

$$\langle|m_{jk}|^2\rangle_0 = (2\beta a_{jk})^{-1} \qquad \langle|w_k|^2\rangle_0 = (2\beta b_k)^{-1}. \tag{19}$$

The averaged model Hamiltonian thus becomes

$$\langle\mathcal{H}_0\rangle_0 = \sum_{jk} a_{jk}\langle|m_{jk}|^2\rangle_0 + \sum_k b_k\langle|w_k|^2\rangle_0 = \frac{1}{2\beta}\sum_{jk} 1 + \frac{1}{2\beta}\sum_k 1. \tag{20}$$

The powers of the fluctuations, $m_j^2(\boldsymbol{R}) = \sum_k |m_{jk}|^2$ and $w_j^2(\boldsymbol{R}) = \sum_k |w_k|^2$, are calculated to be

$$\langle m_j^{2n}(\boldsymbol{R})\rangle_0 = (2n-1)!!\tilde{m}_j^{2n} \tag{21}$$

$$\langle w^{2n}(\boldsymbol{R})\rangle_0 = (2n-1)!!\tilde{w}^{2n} \tag{22}$$

where

$$\tilde{m}_j^2 \equiv \sum_k \langle|m_{jk}|^2\rangle_0 \tag{23}$$

and

$$\tilde{w}^2 \equiv \sum_k \langle|w_k|^2\rangle_0. \tag{24}$$

For the average of Φ_Q, one uses (8), obtaining

$$\Big\langle \sum_{\boldsymbol{R}'} J(\boldsymbol{R}-\boldsymbol{R}')m_j^{2n+1}(\boldsymbol{R})m_j(\boldsymbol{R}')\Big\rangle_0 = (2n+1)!!(\tilde{m}_j^2)^n\tilde{d}_{nj}^2 \tag{25}$$

where

$$\tilde{d}_{nj}^2 \equiv \sum_k J_n(\boldsymbol{k})\langle|m_{jk}|^2\rangle_0. \tag{26}$$

Since the magnetization $\boldsymbol{M}(\boldsymbol{R})$ is composed of the average magnetization $\tilde{\boldsymbol{M}}$ and the components of fluctuations $m_j(\boldsymbol{R})$, the thermal average $\langle\boldsymbol{M}^{2n}(\boldsymbol{R})\rangle_0$ is given by a polynomial in powers of $\langle|m_{Xk}|^2\rangle_0$, $\langle|m_{Yk}|^2\rangle_0$, $\langle|m_{Zk}|^2\rangle_0$, and M^2. In particular, for the ferromagnetic case and the antiferromagnetic case, where the magnetization is given by (2) and (3), respectively, the average values of the two transverse fluctuations, m_{Xk} and m_{Yk}, are degenerate, and we define transverse fluctuations by $\langle|m_{Tk}|^2\rangle_0 \equiv \langle|m_{Xk}|^2\rangle_0 = \langle|m_{Yk}|^2\rangle_0$, and longitudinal fluctuations by $\langle|m_{Lk}|^2\rangle_0 \equiv \langle|m_{Zk}|^2\rangle_0$. Then we express the thermal average $\langle\boldsymbol{M}^{2n}(\boldsymbol{R})\rangle_0$ in terms of powers of $\tilde{m}_T^2$, $\tilde{m}_L^2$, and M^2:

$$\langle\boldsymbol{M}^{2n}(\boldsymbol{R})\rangle_0 = \langle(\boldsymbol{M}_G + m(\boldsymbol{R}))^{2n}\rangle_0 = \sum_{\mu+t+l=n} F_{\mu tl}M^{2\mu}\tilde{m}_T^{2t}\tilde{m}_L^{2l} \tag{27}$$

where $\tilde{m}_T^2$ and $\tilde{m}_L^2$ are defined by (23) using $j = T$ and $j = L$, respectively. For the thermal average involving the exchange-coupling terms, we obtain

$$\Big\langle \sum_{\boldsymbol{R}'} J_n(\boldsymbol{R}-\boldsymbol{R}')M_j^{2n+1}(\boldsymbol{R})M_j(\boldsymbol{R}')\Big\rangle_0 = \sum_{\mu+t+l=n} F_{\mu tl}M^{2\mu}\tilde{m}_T^{2t}\tilde{m}_L^{2l}(\lambda_{T\mu t}\tilde{d}_{nT}^2 + \lambda_{L\mu l}\tilde{d}_{nL}^2). \tag{28}$$

The polynomial coefficients $F_{\mu tl}$, $\lambda_{T\mu t}$, and $\lambda_{L\mu l}$ depend on the form of the macroscopic magnetization $\tilde{\boldsymbol{M}}$ of (1). For the ferromagnet, equation (2), they are calculated as

$$F^F_{\mu tl} = \frac{(\mu+t+l)!}{\mu!t!l!}\frac{2^t t!(2\mu+2l-1)!!}{(2\mu-1)!!} \qquad \lambda^F_{T\mu t} = 2t+2 \qquad \lambda^F_{L\mu l} = 2\mu+2l+1 \tag{29}$$

and for an antiferromagnetic spin-spiral configuration, equation (3), one obtains

$$F^A_{\mu tl} = \frac{(\mu+t+l)!}{\mu!t!l!}\frac{2^t(\mu+t)!(2l-1)!!}{\mu!} \qquad \lambda^A_{T\mu t} = 2\mu+2t+2 \qquad \lambda^A_{L\mu l} = 2l+1. \tag{30}$$

In the same way, the thermal averages of powers of the volume are calculated as

$$\langle V^m(\boldsymbol{R})\rangle_0 = \langle (V+w(\boldsymbol{R}))^m\rangle_0 = \sum_{v+2u=m} G_{vu} V^v \tilde{w}^{2u} \tag{31}$$

where the binomial coefficients G_{vu} are given by

$$G_{vu} = \frac{(v+2u)!}{v!(2u)!}(2u-1)!!. \tag{32}$$

A detailed calculation of the coefficients $F_{\mu tl}$, $\lambda_{T\mu t}$, $\lambda_{L\mu t}$, and G_{vu} can be found in [27].

Finally, using equations (27), (28), and (31), we obtain for the thermal average of the Hamiltonian $\mathcal{H}$, equation (5),

$$\begin{aligned}\langle\mathcal{H}\rangle_0 &= \sum_{n,m} A_{nm}\langle \boldsymbol{M}^{2n}(\boldsymbol{R})\rangle_0\langle V^m(\boldsymbol{R})\rangle_0 + \sum_n \Big\langle \sum_{\boldsymbol{R}'} J_n(\boldsymbol{R}-\boldsymbol{R}') M_j^{2n+1}(\boldsymbol{R}) M_j(\boldsymbol{R}')\Big\rangle_0 \\ &= \sum_{\substack{\mu tl \\ n=\mu+t+l}} F_{\mu tl} M^{2\mu} \tilde{m}_T^{2t}\tilde{m}_L^{2l}\Big(\sum_{\substack{vu \\ m=v+2u}} A_{nm}G_{vu}V^v\tilde{w}^{2u} + \lambda_{T\mu t}\tilde{d}^2_{nT} + \lambda_{L\mu l}\tilde{d}^2_{nL}\Big).\end{aligned} \tag{33}$$

This, together with (19), completes the specification of the free energy, equation (16). Tables for the coefficients $F_{\mu tl}$ and G_{vu} are given in the appendix.

2.5. Self-consistency equations

The thermal equilibrium values for M and V as well as their fluctuations $\langle|m_{j\boldsymbol{k}}|^2\rangle_0$ and $\langle|w_{\boldsymbol{k}}|^2\rangle_0$ are calculated by requiring that the quantities $a_{j\boldsymbol{k}}$, $b_{\boldsymbol{k}}$, M, and V minimize the free energy $\mathcal{F}_{SF}$, i.e.

$$0 = \frac{\partial\mathcal{F}_{SF}}{\partial M} \qquad 0 = \frac{\partial\mathcal{F}_{SF}}{\partial V} \qquad 0 = \frac{\partial\mathcal{F}_{SF}}{\partial a_{j\boldsymbol{k}}} \qquad 0 = \frac{\partial\mathcal{F}_{SF}}{\partial b_{\boldsymbol{k}}}. \tag{34}$$

Because of (19) we may replace the derivatives with respect to $a_{j\boldsymbol{k}}$ and $b_{\boldsymbol{k}}$ by derivatives with respect to $\langle|m_{j\boldsymbol{k}}|^2\rangle_0$ and $\langle|w_{\boldsymbol{k}}|^2\rangle_0$. Furthermore, using the identities

$$\partial\langle\mathcal{H}\rangle_0/\partial\langle|m_{j\boldsymbol{k}}|^2\rangle_0 = \partial\langle\mathcal{H}\rangle_0/\partial\langle\tilde{m}_j^2\rangle_0 + \sum_n J_n(\boldsymbol{k})\,\partial\langle\mathcal{H}\rangle_0/\partial\langle\tilde{d}^2_{nj}\rangle_0$$

and

$$\partial\langle\mathcal{H}\rangle_0/\partial\langle|m_{T\boldsymbol{k}}|^2\rangle_0 = 2\,\partial\langle\mathcal{H}\rangle_0/\partial\langle|m_{X\boldsymbol{k}}|^2\rangle_0$$

we obtain the following self-consistency equations:

$$0 = \frac{\partial \langle \mathcal{H} \rangle_0}{\partial M} \tag{35}$$

$$0 = \frac{\partial \langle \mathcal{H} \rangle_0}{\partial V} \tag{36}$$

$$\frac{2}{2\beta \langle |m_{Tk}|^2 \rangle_0} = \frac{\partial \langle \mathcal{H} \rangle_0}{\partial \tilde{m}_T^2} + \sum_n J_n(\boldsymbol{k}) \frac{\partial \langle \mathcal{H} \rangle_0}{\partial \tilde{d}_{nT}^2} \tag{37}$$

$$\frac{1}{2\beta \langle |m_{Lk}|^2 \rangle_0} = \frac{\partial \langle \mathcal{H} \rangle_0}{\partial \tilde{m}_L^2} + \sum_n J_n(\boldsymbol{k}) \frac{\partial \langle \mathcal{H} \rangle_0}{\partial \tilde{d}_{nL}^2} \tag{38}$$

$$\frac{1}{2\beta \langle |w_{\boldsymbol{k}}|^2 \rangle_0} = \frac{\partial \langle \mathcal{H} \rangle_0}{\partial \tilde{w}^2}. \tag{39}$$

These equations are easily written out explicitly, and enable us to calculate self-consistently the quantities M, V, $\langle |m_{Tk}|^2 \rangle_0$, $\langle |m_{Lk}|^2 \rangle_0$, and $\langle |w_{\boldsymbol{k}}|^2 \rangle_0$ which determine the thermal equilibrium of the system.

In the paramagnetic case, the average magnetization vanishes, i.e. $M = 0$, and all components of the fluctuations are degenerate, $\langle |m_{Pk}|^2 \rangle_0 \equiv \langle |m_{Xk}|^2 \rangle_0 = \langle |m_{Yk}|^2 \rangle_0 = \langle |m_{Zk}|^2 \rangle_0$. In this case the mean value of the Hamiltonian can be simplified:

$$\langle \mathcal{H}^{(P)} \rangle_0 = \sum_n (2n+1)!! \tilde{m}_P^{2n} \Bigg(\sum_{\substack{mvu \\ v+2u=m}} A_{nm} G_{vu} V^v \tilde{w}^{2u} + (2n+3) \tilde{d}_{nP}^2 \Bigg) \tag{40}$$

and the self-consistency equations of the paramagnetic case are given by equations (36), (39), and

$$\frac{3}{2\beta \langle |m_{Pk}|^2 \rangle_0} = \frac{\partial \langle \mathcal{H} \rangle_0}{\partial \tilde{m}_P^2} + \sum_n J_n(\boldsymbol{k}) \frac{\partial \langle \mathcal{H} \rangle_0}{\partial \tilde{d}_{nP}^2}. \tag{41}$$

The inverse magnetic susceptibility $\chi_j^{-1}(\boldsymbol{k})$ can be calculated easily from the second derivative of the free energy:

$$\chi_j^{-1}(\boldsymbol{k}) = \frac{\partial^2 \mathcal{F}_{SF}}{\partial m_{j(+\boldsymbol{k})} \, \partial m_{j(-\boldsymbol{k})}} = \frac{1}{\beta \langle |m_{j\boldsymbol{k}}|^2 \rangle_0} = 2a_{j\boldsymbol{k}}. \tag{42}$$

Evidently, the best variational coefficients of the free energy, equation (16), are given by the inverse susceptibility, $a_{j\boldsymbol{k}} = \chi_j^{-1}(\boldsymbol{k})/2$, whose $\boldsymbol{k}$-dependence is in first order given by the Fourier coefficients of the exchange constants, $\chi_j^{-1}(\boldsymbol{k}) = \chi_j^{-1}(\boldsymbol{0}) + 2J_0(\boldsymbol{k})$.

3. Calculational details

Our band-structure calculations presented here are performed with the augmented-spherical-wave (ASW) method [28], which is based on the local spin-density approximation (LSDA) to the density functional theory [29–31]. In particular, using the non-collinear fixed-spin-moment method [25, 26] we are able to perform constrained-moments calculations of non-collinear spin arrangements. This enables us to compute electronic properties of different magnetic configurations, i.e. for any choice of the magnitudes of the moments *and* their directions, and to determine their mutual range of stability by comparing the resulting total energies.

4. Results

4.1. γ-Fe

In recent years, γ-Fe has received much attention [8, 9, 32], because, among other things, many iron alloys showing anomalous magneto-elastic properties are based on the fcc structure of γ-Fe—for instance $Fe_{65}Ni_{35}$, $Fe_{72}Ni_{28}$, and Fe–Mn alloys [3]. In nature, γ-Fe exists only as a high-temperature phase, whereas at low temperatures it can be stabilized for instance by small amounts of Co [33, 34].

Experimental investigations [33, 34] have shown, that, at certain volumes, γ-Fe has an antiferromagnetic ground state and, due to its frustration in the fcc lattice, assumes a non-collinear spin configuration. These results are confirmed by theoretical work [35], including band-structure calculations [25, 36, 37]. In recent work by Acet *et al* [32] magneto-elastic properties of γ-Fe were investigated, and an anomalously high thermal expansion coefficient was observed which deviates significantly from the normal Grüneisen behaviour. This so-called anti-Invar behaviour is explained by the coexistence of an antiferromagnetic low-spin (LS) state at small volume and a ferromagnetic high-spin (HS) state at large volume; see e.g. [38]. Thermal occupation of the HS state results in a large magnetic contribution to the volume expansion. A detailed theoretical study of the different collinear and non-collinear spin configurations of γ-Fe was given previously [26]. However, a thermodynamic treatment is still lacking. We present one here, based on the self-consistent spin-fluctuation theory of section 2.

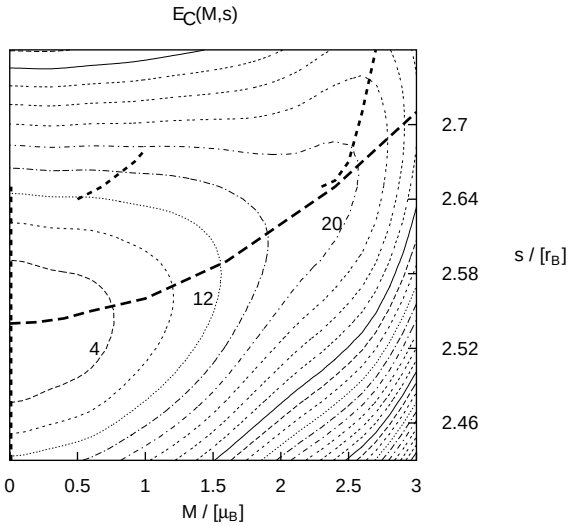

Figure 1. γ-Fe: the collinear contribution to the total energy $E_C(M, V)$ in mRyd per unit cell. The distance between nearest contour lines is 4 mRyd. The locus of $b = 0$ (- - -) and $p = 0$ (– – –) (see the text) is also given.

In figures 1 and 2 we plot for γ-Fe the total-energy contributions, E_C and E_Q, which add up to the total energy, $E(\tilde{\boldsymbol{M}}, V) = E_C(M, V) + E_Q(M, \boldsymbol{q}, \theta)$. The energy dependence on the volume V (or the corresponding Wigner–Seitz radius s: $V = (4\pi/3)s^3$) and the magnetic moment M of $E_C(M, s)$ is shown in figure 1, which reveals that the ground state of γ-Fe is non-magnetic, corresponding to the minimum of $E_C(M, s)$ at $M_0 = 0\mu_B$ and $s_0 = 2.56r_B$, where r_B denotes the Bohr radius. Furthermore, the locus of zero derivatives,

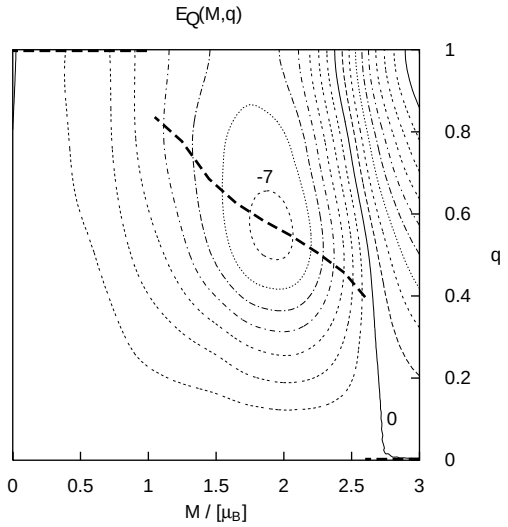

Figure 2. γ-Fe: the non-collinear contribution to the total energy $E_Q(M, \boldsymbol{q})$ in mRyd per unit cell for wave vectors $\boldsymbol{q} = (0, 0, q)2\pi/a$. The distance between nearest contour lines is 1 mRyd. The line (- - -) depicts those wave vectors $\boldsymbol{q}$ which minimize E_Q for fixed values of M.

i.e. $b = \partial E_C/\partial M = 0$ (the heavy dotted line) and $p = \partial E_C/\partial V = 0$ (the heavy dashed line) are drawn, which indicate an additional high-spin state of higher total energy having a magnetization of $M = 2.5\mu_B$ at a Wigner–Seitz radius of $s = 2.65r_B$.

In figure 2 the total-energy contribution $E_Q(M, \boldsymbol{q})$ describes the total-energy costs of a spin-spiral arrangement defined by the vector $\boldsymbol{q}$ and the magnitude of the moment M; see (3). Here the heavy dashed line denotes the particular wave vector $\boldsymbol{q}_0$ which minimizes E_Q for a given value of M. It is seen that at small values of the magnetization ($M < 2.5\mu_B$) the moments tend to order antiferromagnetically ($\boldsymbol{q} \neq 0$), whereas at large values ($M > 2.5\mu_B$) the ferromagnetic configuration ($\boldsymbol{q} = 0$) is favoured.

This complex behaviour of the energy surfaces shown in figure 1 and figure 2 gives rise to the need to use a large number of terms in the Taylor series expansion of the total energy $E(V, M, \boldsymbol{q})$, given by (4). In particular, for γ-Fe, terms up to M^8 and V^4 in $E_C(M, V)$ and $E_Q(M, \boldsymbol{q})$ must be employed. The $\boldsymbol{q}$-dependence of the latter is approximated by a set of 20 vectors $\boldsymbol{q}$, spread homogeneously over the irreducible part of the Brillouin zone.

With this numerical input and the equations (35)–(39), the fluctuations $m_{j\boldsymbol{k}}$ and $w_{\boldsymbol{k}}$ as well as the equilibrium values of M and V were calculated self-consistently, scanning a large temperature range. Our results for γ-Fe are shown in figure 3, where we plot the paramagnetic fluctuations, $\tilde{m}_P^2 = \sum_{\boldsymbol{k}} \langle |m_{P\boldsymbol{k}}|^2 \rangle_0$, as a function of T, from which the magnitude of the local moment M_s is calculated as

$$M_s = \sqrt{3\tilde{m}_P^2}.$$

Also given are the inverse susceptibilities $\chi^{-1}(\boldsymbol{k}) = (\beta \langle |m_{P\boldsymbol{k}}|^2 \rangle_0)^{-1}$ for two different $\boldsymbol{k}$-vectors, χ^{-1}(F) for $\boldsymbol{k} = (0, 0, 0)$ (the uniform susceptibility or ferromagnetic mode) and χ^{-1}(A) for $\boldsymbol{k} = (0, 0, 2\pi/a)$ (the staggered susceptibility or antiferromagnetic mode).

At low temperatures, χ^{-1}(F) is about ten times larger than χ^{-1}(A), whereas with increasing temperatures, χ^{-1}(A) increases more quickly than χ^{-1}(F). Thus at low temperatures, predominantly antiferromagnetic fluctuations forming small local magnetic

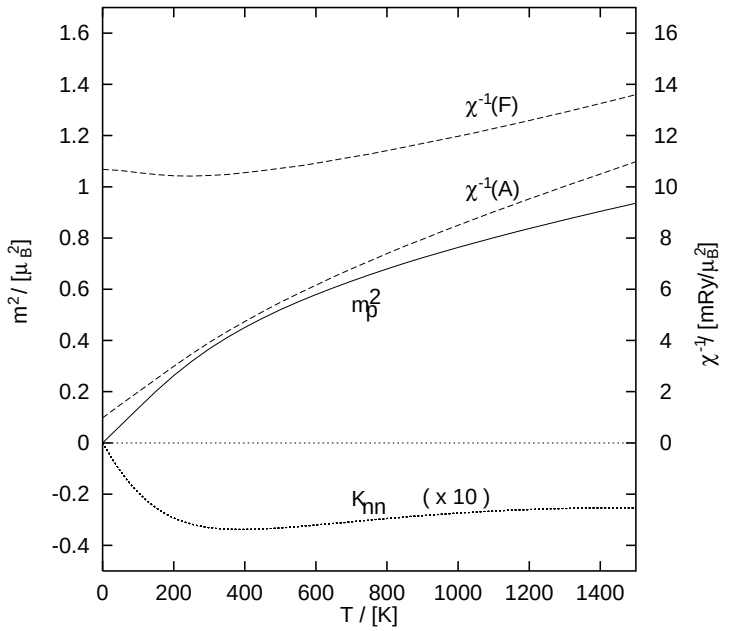

Figure 3. Paramagnetic fluctuations ($\tilde{m}_p^2/\mu_B^2$), the susceptibilities χ^{-1}(F) and χ^{-1}(A) in mRyd/μ_B^2, and the magnetic correlation of nearest neighbours K_{nn}/μ_B^2, scaled by a factor of 10, for γ-Fe, as a function of temperature.

moments ($M_s < 1.5\mu_B$) are excited, whereas at higher temperatures a large occupation of ferromagnetic fluctuations occurs, leading to $M_s > 1.5\mu_B$; see also figure 2. This is shown even more convincingly by the magnetic correlation between nearest-neighbour sites, defined by

$$\kappa_{nn} = \langle \boldsymbol{M}(\boldsymbol{0}) \cdot \boldsymbol{M}(\boldsymbol{d}_{nn}) \rangle_0 = 3 \sum_{\boldsymbol{k}} \cos(\boldsymbol{k} \cdot \boldsymbol{d}_{nn}) \langle |m_{P\boldsymbol{k}}|^2 \rangle_0$$

where $\boldsymbol{d}_{nn}$ is the distance between nearest neighbours. The correlation function, $\kappa_{nn}(T)$, is also shown in figure 3, where at $T \simeq 390$ K we observe a maximal antiferromagnetic coupling, noticeable by the minimum of $\kappa_{nn}(T)$.

In figure 4 we show the magnetic contribution to the temperature dependence of the volume V and the thermal expansion coefficient, $\alpha = (1/3V)\mathrm{d}V/\mathrm{d}T$. Our calculated curves (calc.) are compared with experimental data (exp.) of Acet *et al* [32]. The increase of the volume is brought about by a thermal occupation of high-spin states associated with large volumes, as shown in figure 1. It is seen that for $T > 600$ K the experimental thermal expansion coefficient decreases slightly with increasing temperature, which is due to its magnetic contribution. This behaviour is in agreement with our calculations, and may be explained by the fact that with increasing temperature the increase in the fluctuations becomes smaller, leading to a smaller but still positive value of $\alpha(T)$ even for temperatures above 1000 K. In a large temperature range our calculated thermal expansion coefficient is somewhat smaller than the experimental one but still in reasonable agreement, whereas near $T = 0$ we obtain a non-vanishing $\alpha(T)$. This incorrect behaviour is due to our treating the spin fluctuations as classical variables, which does not describe properly the freezing out of the spin excitations at $T \to 0$.

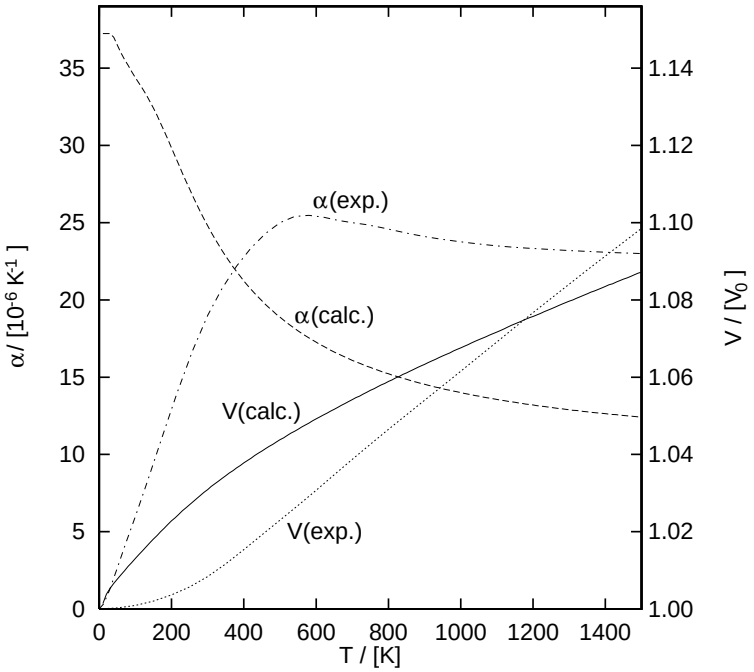

Figure 4. The relative volume ($V(T)/V_0$) and linear expansion coefficient ($\alpha/10^{-6}$ K^{-1}) of γ-Fe as a function of the temperature T/K: The calculated curves (calc.) are compared with experimental data (exp.) of Acet *et al* [32].

4.2. Fe_3Pt

Fe_3Pt is one of the best-known Invar alloys. It is based on the fcc structure of γ-Fe, where one of four Fe atoms in the cubic unit cell is replaced by Pt. Similar to the case for γ-Fe, the Invar effect of Fe_3Pt is due to the coexistence of a HS state at large volume and a LS state at small volume, but contrary to the case for γ-Fe, the ground state is now the ferromagnetic HS state; this is brought about by the larger atomic volume of Pt. Thus, at finite temperatures the increasing occupation of LS states leads to a large negative magnetic contribution to the expansion coefficient, which in Fe_3Pt is observed to be 3×10^{-5} K^{-1} near T_C.

In figure 5 we show the collinear contribution $E_C(M, V)$ to the total energy as a function of the Wigner–Seitz radius ($s = s_{\mathrm{Fe}} = s_{\mathrm{Pt}}$) and the average magnetic moment per atom ($M = \frac{3}{4}M_{\mathrm{Fe}} + \frac{1}{4}M_{\mathrm{Pt}}$). The ferromagnetic ground state is found at the crossing point of the curves $b = 0$ (the heavy dotted line) and $p = 0$ (the heavy dashed line) at a Wigner–Seitz radius of $s_0 = 2.79r_B$. Here at the iron sites we observe a magnetic moment $M_{\mathrm{Fe}} = 2.67\mu_B$, and at the platinum site $M_{\mathrm{Pt}} = 0.27\mu_B$ which gives an average ground-state moment of $M_0 = 2.07\mu_B$ per atom.

In figure 6 the non-collinear contribution $E_Q(M, \boldsymbol{q})$ is shown for wave vectors $\boldsymbol{q} = q(1, 1, 1)2\pi/a$. It is seen that like γ-Fe, Fe_3Pt orders ferromagnetically at large values of the magnetic moment ($M > 1.9\mu_B$), and at small values a non-collinear antiferromagnetic order is favoured.

Again, for the calculations of spin fluctuations in Fe_3Pt, the parameters of the Hamiltonian are extracted from the total-energy curves shown in figures 5 and 6. Here,

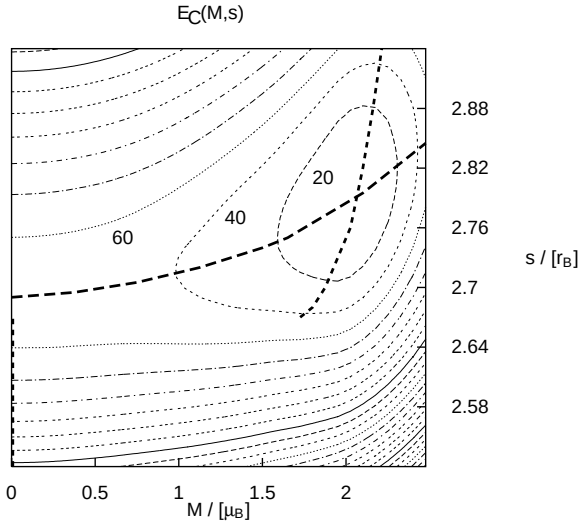

Figure 5. Fe_3Pt: the collinear contribution to the total energy $E_C(M, V)$ in mRyd per unit cell. The distance between nearest contour lines is 20 mRyd. The locus of $b = 0$ (- - -) and $p = 0$ (– – –) (see the text) is also given.

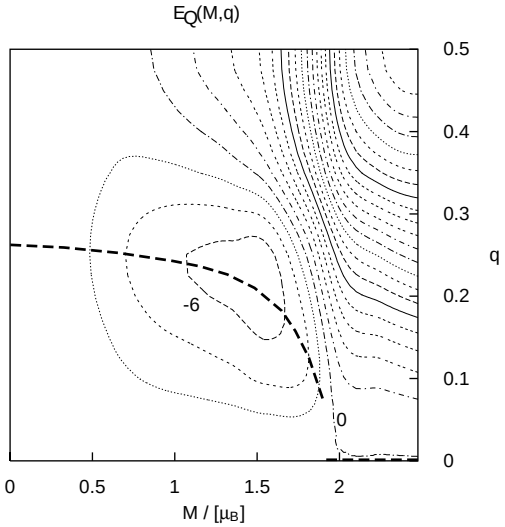

Figure 6. Fe_3Pt: the non-collinear contribution to the total energy $E_Q(M, \boldsymbol{q})$ in mRyd per unit cell for wave vectors $\boldsymbol{q} = (q, q, q)2\pi/a$. The distance between nearest contour lines is 2 mRyd. The line (- - -) depicts those wave vectors $\boldsymbol{q}$ which minimize E_Q for fixed values of M.

in analogy to earlier work [12, 19, 20, 39], we do not account for different volumes and magnetic moments of Fe and Pt sites, and the total energy is written as a function of the average values of M and V per atomic site. As for γ-Fe, terms up to M^8 and V^4 in E_C and E_Q are employed. For Fe_3Pt, the self-consistency equations, (35)–(39), yield a Curie temperature of $T_C = 504$ K, which is somewhat larger than the experimental values of 430 K for ordered $Fe_{75}Pt_{25}$ [40] and 390 K for disordered $Fe_{72}Pt_{28}$ [41].

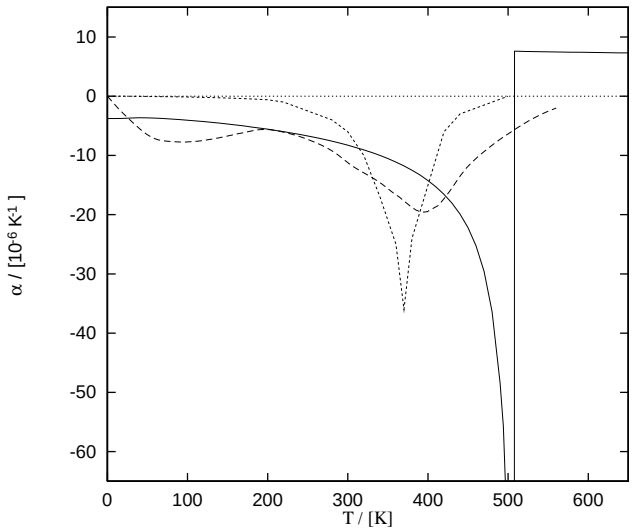

Figure 7. The magnetic contribution to the thermal expansion coefficient ($\alpha/10^{-6}$ K^{-1}) of Fe_3Pt: the calculated curve (—) is compared with the experimental data of Sumiyama *et al* (- - -: ordered $Fe_{75}Pt_{25}$ [40, 42] and – – –: disordered $Fe_{72}Pt_{28}$ [41, 42]). Note that the experimental values of T_C are 430 K for ordered $Fe_{75}Pt_{25}$ and 390 K for disordered $Fe_{72}Pt_{28}$.

Next, we show in figure 7 the calculated thermal expansion coefficient $\alpha = (1/3V)\mathrm{d}V/\mathrm{d}T$ of Fe_3Pt, comparing it with the experimental curves for the magnetic contribution to the expansion coefficient of ordered $Fe_{75}Pt_{25}$ (the dashed line; reference [40]) and disordered $Fe_{72}Pt_{28}$ (the dotted line; reference [41]), taken from Menshikov [42]. Below T_C the absolute value of the calculated expansion coefficient is seen to increase with increasing temperature, having a maximum at $T = T_C$. This behaviour is in reasonable agreement with the peaks in the experimental curve, which occur at temperatures slightly lower than the experimental T_C. This may be attributed to magnetic inhomogeneities, since even in the ordered structure a small amount of displaced Fe and Pt sites is observed. The singularity of $\alpha(T)$ at $T = T_C$ is due to a strong coupling between the volume V and the magnetization M accompanied by an unphysical singularity in the derivative $\mathrm{d}M/\mathrm{d}T$ at T_C which can be traced back to the mean-field approximation used. In the paramagnetic phase the calculated expansion coefficient is positive and nearly constant with temperature, which is due to the proportionality of the volume and the local magnetization and an approximately linear increase of the paramagnetic fluctuations $\tilde{m}_p^2(T)$; compare also figure 9, later.

4.3. γ-Mn

Like γ-Fe, pure γ-Mn is only observed as a high-temperature phase, but can be stabilized by small amounts of other materials, for example Fe or Cu at low temperatures, and is found to order antiferromagnetically below a Néel temperature, T_N, of about 540 K [43].

Again, γ-Mn shows an anomalous behaviour of the thermal expansion coefficient—see e.g. [44, 45]—but, contrary to γ-Fe or Fe_3Pt, below T_N γ-Mn is observed to be tetragonally distorted with a c/a ratio of $c/a \simeq 0.945$ at $T = 0$ K [43]. This lattice distortion is due to the tetragonally reduced symmetry of the antiferromagnetic spin configuration, described by a wave vector $\boldsymbol{q} = (0, 0, 2\pi/c)$ along the c-axis.

It should be mentioned here that in some cases a distorted structure may not be described

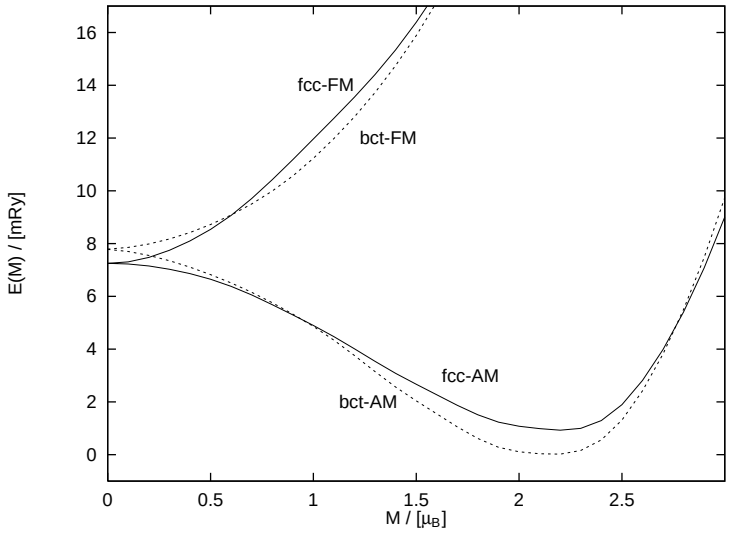

Figure 8. The calculated total energy E in mRyd for the ferromagnetic (FM) and the antiferromagnetic (AM) phases of cubic (fcc) and tetragonal distorted (bct) γ-Mn as functions of the magnetic moment M in μ_B.

correctly within the atomic sphere approximation as used in the ASW method, in particular if the arrangement of orbitals leads to an aspherical charge density. This is not the case in γ-Mn, where the lattice distortion is solely caused by a difference in magnetic pressure between parallel- and antiparallel-ordered Mn atoms, and does not lead to inequivalent Mn sites.

In figure 8 the total-energy curves $E(M)$ calculated for the ferromagnetic (FM) and the antiferromagnetic (AM) phases of the cubic (fcc) and the tetragonally distorted (bct) structure of γ-Mn are shown. In both structures the minimum of energy is given by the antiferromagnetic phase, having a magnetic moment $M_0 \simeq 2.15\mu_B$. Here it is seen that the bct curve is lower in energy for values $1.0\mu_B < M < 2.8\mu_B$; thus the ground state is tetragonally distorted, whereas for small values $M < 1.0\mu_B$ the fcc structure is favourable. Furthermore, it is seen that for both structures the ferromagnetic configuration cannot be stabilized, since the energy increases rapidly with increasing magnitude of the moment M.

Due to the antiferromagnetic ground state which is defined by (3), where $\boldsymbol{q} = (0, 0, 2\pi/c)$, we now obtain spin fluctuations which differ from those in a ferromagnet. In particular, the coupling between $\tilde{\boldsymbol{M}}$ and the longitudinal fluctuations $\tilde{m}_l^2$, which in the ferromagnet is weaker than that between $\tilde{\boldsymbol{M}}$ and the transverse fluctuations $\tilde{m}_t^2$, is now stronger in the antiferromagnet. This may be proved by comparing (29) with (30), and is clearly seen in figure 9, where we collect together our results for γ-Mn. Shown here are $\tilde{m}_t^2$, $\tilde{m}_l^2$, $\tilde{m}_p^2$ (in units of M_0^2), the magnetization M, and the local magnetic moment

$$M_s = \sqrt{M^2 + 2\tilde{m}_t^2 + \tilde{m}_l^2}$$

(in units of M_0), which should be compared with our results for fcc Ni obtained previously [24]. For the Néel temperature we obtain $T_N = 446$ K, which is smaller than the experimental value (540 K).

To take into account the effect of the lattice distortion, we treat the volume dependence by now expressing the total energy as a function of the distortion parameter $\delta = c/a - 1$,

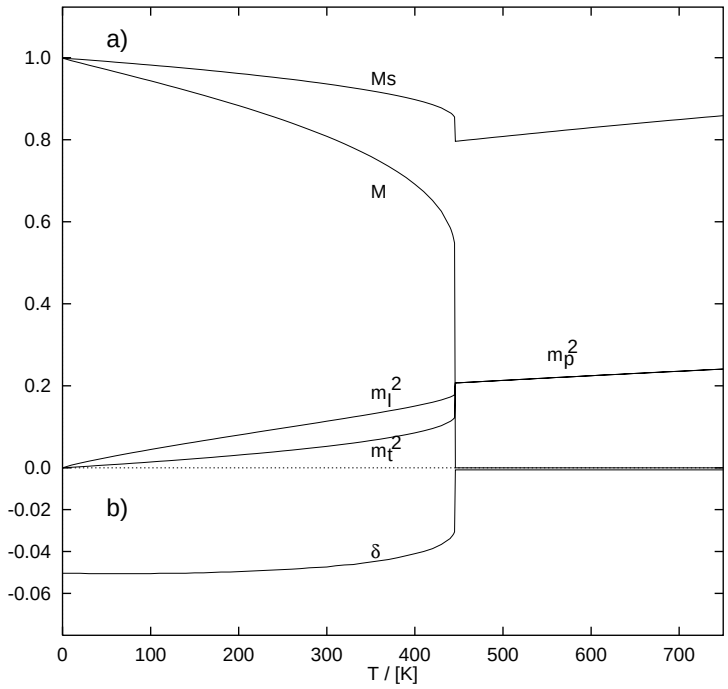

Figure 9. (a) The fluctuations $\tilde{m}_t^2$, $\tilde{m}_l^2$, and $\tilde{m}_p^2$ (in M_0^2), the magnetization M, and the local magnetic moment M_s (in M_0) of γ-Mn; (b) the distortion parameter $\delta = c/a - 1$ as function of the temperature T/K.

and add the following contribution to the total energy of equation (4):

$$E_{\mathrm{dist}}(M, \delta) = \delta(\zeta_0 + \zeta_1 M^2 + \zeta_2 M^4) + \delta^2(\eta_0 + \eta_1 M^2 + \eta_2 M^4).$$

The coefficients ζ_0, ζ_1, ζ_2, η_0, η_1, and η_2 are evaluated by fitting $E_{\mathrm{dist}}(M, \delta)$ to the computed total-energy curves; see also figure 8.

The calculated distortion $\delta(T)$ is shown in figure 9, where it is seen that δ decreases with increasing temperature and vanishes in the paramagnetic state ($T > T_N$). Furthermore, at $T = T_N$ a discontinuity of the magnetization is observed, which, most probably, is a consequence of our mean-field approximation and the quadratic form of the model Hamiltonian; see also [15, 22].

5. Conclusion

In summary, we have presented a first-principles theory for estimating finite-temperature properties of itinerant-electron systems. We obtained all of the parameters entering a Ginzburg–Landau-type Hamiltonian by means of constrained-ground-state calculations using the local density functional approximation. The gradient term in the Ginzburg–Landau Hamiltonian was replaced by an exchange term $J(\boldsymbol{k})$ which describes the excitation energies of spin fluctuations, and was also obtained by constrained-ground-state calculations using spin-spiral configurations. Furthermore, the detailed calculations of the thermal averages of the Hamiltonian are accomplished by Taylor series expansions in the volume, the magnetization, and the exchange parameters. This general treatment allows us to apply our theory to systems with ferromagnetic, antiferromagnetic, or non-collinear ground states,

and to materials with complex energy surfaces like Invar or anti-Invar alloys, enabling us to investigate magneto-volume effects in γ-Fe, Fe_3Pt, and γ-Mn.

As shown in previous investigations [25, 26, 10, 11], the anharmonicity of the volume in γ-Fe and Fe_3Pt is properly reflected by the calculated *energy landscapes*, $E(M, V)$ (figures 1 and 5), and leads to an anti-Invar behaviour in γ-Fe where the LS state is lower in energy than the HS state, and to the Invar effect in Fe_3Pt where the ground state is the HS state. Together with the magnetic excitation energies, extracted by means of calculations of non-collinear *'frozen-spin-wave'* configurations (figures 2 and 6), our total-energy calculations result in reasonable *ab initio* values for the magneto-elastic properties for γ-Fe and Fe_3Pt, and give an explanation of the atypical behaviour in γ-Fe, which shows AM features at low temperatures and FM behaviour at higher temperatures. Since the thermodynamical description of fluctuations is performed within a quadratic (Gaussian) approximation of the partition function, we cannot reproduce all of the features of the thermodynamics entirely satisfactorily—which in particular leads to discrepancies at the transition temperature and for $T \to 0$. However, our estimates of the Curie temperatures given previously [24], as well as the Curie and Néel temperatures given here, and the qualitatively correct description of the Invar effect in Fe_3Pt and the anti-Invar effect in γ-Fe, must be called reasonably successful.

Thus we may conclude that our total-energy density functional calculations provide a good basis on which to estimate first-principles finite-temperature properties, although there is room for much improvement.

Acknowledgments

We would like to express our thanks to M Schröter for interesting and helpful discussions. This work was partially supported by the Deutsche Forschungsgemeinschaft, SFB 252, Darmstadt, Frankfurt, Mainz.

Table A1. Polynomial coefficients $F^F_{\mu t l}$ of the ferromagnet up to powers $n = \mu + t + l = 4$.

$n = \mu + t + l$		$l = 0$	$l = 1$	$l = 2$	$l = 3$	$l = 4$
$n = 0$	$t = 0$	1				
$n = 1$	$t = 0$	1	1			
	$t = 1$	2				
$n = 2$	$t = 0$	1	6	3		
	$t = 1$	4	4			
	$t = 2$	8				
$n = 3$	$t = 0$	1	15	45	15	
	$t = 1$	6	36	18		
	$t = 2$	24	24			
	$t = 3$	48				
$n = 4$	$t = 0$	1	28	210	420	105
	$t = 1$	8	120	360	120	
	$t = 2$	48	288	144		
	$t = 3$	192	192			
	$t = 4$	384				

Appendix

The polynomial coefficients $F_{\mu tl}$ are shown for the ferromagnetic configuration ($F^F_{\mu tl}$)—see (29)—in table A1 and for the antiferromagnetic spin-spiral configuration ($F^A_{\mu tl}$)—see (30)—in table A2. Furthermore, the binomial coefficients G_{vu} of equation (32) are given in table A3.

Table A2. Polynomial coefficients $F^A_{\mu tl}$ of the antiferromagnet up to the powers $n = \mu+t+l = 4$.

$n=\mu+t+l$		$l=0$	$l=1$	$l=2$	$l=3$	$l=4$
$n=0$	$t=0$	1				
$n=1$	$t=0$	1	1			
	$t=1$	2				
$n=2$	$t=0$	1	2	3		
	$t=1$	8	4			
	$t=2$	8				
$n=3$	$t=0$	1	3	9	15	
	$t=1$	18	24	18		
	$t=2$	72	24			
	$t=3$	48				
$n=4$	$t=0$	1	4	18	60	105
	$t=1$	32	72	144	120	
	$t=2$	288	288	144		
	$t=3$	768	192			
	$t=4$	384				

Table A3. Binomial coefficients G_{vu} up to the powers $m = v+2w = 6$.

$m=v+2w$	$w=0$	$w=1$	$w=2$	$w=3$
$v=0$	1	1	3	15
$v=1$	1	3	15	
$v=2$	1	6	45	
$v=3$	1	10		
$v=4$	1	15		
$v=5$	1			
$v=6$	1			

References

[1] Guillaume C E 1897 *C. R. Acad. Sci., Paris* **125** 235
[2] Wassermann E F 1989 *Phys. Scr.* T **25** 209
[3] Wassermann E F 1990 *Ferromagnetic Materials* vol 5, ed K H J Buschow and E P Wohlfarth (Amsterdam: North-Holland)
[4] Campbell I A and Creuzet G 1987 *Metallic Magnetism* ed H Capellmann (Berlin: Springer)
[5] Weiss R J 1963 *Proc. Phys. Soc.* **82** 281
[6] Williams A R, Moruzzi V L, Gelatt C D Jr, Kübler J and Schwarz K 1982 *J. Appl. Phys.* **53** 2019
[7] Williams A R, Moruzzi V L, Gelatt C D Jr and Kübler J 1983 *J. Magn. Magn. Mater.* **31–34** 88
[8] Moruzzi V L, Marcus P M, Schwarz K and Mohn P 1986 *Phys. Rev.* B **34** 1784

[9] Moruzzi V L, Marcus P M and Kübler J 1989 *Phys. Rev.* B **39** 6957
[10] Podgorny M 1989 *Physica* B **161** 105
[11] Podgorny M 1991 *Phys. Rev.* B **43** 11 300
[12] Mohn P, Schwarz K and Wagner D 1989 *Physica* B **161** 153
[13] Mohn P, Schwarz K and Wagner D 1991 *Phys. Rev.* B **43** 3318
[14] Murata K K and Doniach S 1972 *Phys. Rev. Lett.* **29** 285
[15] Lonzarich G G and Taillefer L 1985 *J. Phys. C: Solid State Phys.* **18** 4339
[16] Wagner D and Wohlfarth E P 1986 *Phys. Lett.* **118A** 29
[17] Wohlfarth E P and Mohn P 1988 *Physica* B **149** 145
[18] Entel P and Schröter M 1988 *J. Physique Coll.* **49** 293
[19] Entel P and Schröter M 1989 *Physica* B **161** 160
[20] Schröter M and Entel P 1990 *Physica* B **165** 229
[21] Schröter M and Entel P 1993 *Int. J. Mod. Phys.* B **7** 687
[22] Wagner D 1989 *J. Phys.: Condens. Matter* **1** 4635
[23] Shimizu M 1981 *Phys. Lett.* **81A** 87
[24] Uhl M and Kübler J 1996 *Phys. Rev. Lett.* **77** 334
[25] Uhl M, Sandratskii L M and Kübler J 1992 *J. Magn. Magn. Mater.* **103** 314
[26] Uhl M, Sandratskii L M and Kübler J 1994 *Phys. Rev.* B **50** 291
[27] Uhl M 1995 *Thesis* TH Darmstadt
[28] Williams A R, Kübler J and Gelatt C D Jr 1979 *Phys. Rev.* B **19** 6094
[29] Hohenberg P and Kohn W 1964 *Phys. Rev.* B **136** 864
[30] Kohn W and Sham L J 1965 *Phys. Rev.* A **140** 1133
[31] von Barth U and Hedin L 1972 *J. Phys. C: Solid State Phys.* **5** 1629
[32] Acet M, Zähres H, Wassermann E F and Pepperhoff W 1994 *Phys. Rev.* B **49** 6012
[33] Tsunoda Y 1989 *J. Phys.: Condens. Matter* **1** 10 427
[34] Tsunoda Y and Nicklow R M 1993 *J. Phys.: Condens. Matter* **5** 8999
[35] Hirai K 1992 *J. Magn. Magn. Mater.* **104** 749
[36] Mryasov O N, Liechtenstein A I, Sandratskii L M and Gubanov V A 1991 *J. Phys.: Condens. Matter* **3** 7683
[37] Antropov V P, Katsnelson M I, van Schilfgaarde M and Harmon B N 1996 *Phys. Rev.* B **54** 1019
[38] Moruzzi V L 1990 *Phys. Rev.* B **41** 6939
[39] Schröter M, Entel P and Mishra S G 1990 *J. Magn. Magn. Mater.* **87** 163
[40] Sumiyama K, Emoto Y, Shiga M and Nakamura Y 1981 *J. Phys. Soc. Japan* **50** 3296
[41] Sumiyama K, Shiga M, Morioka M and Nakamura Y 1979 *J. Phys. F: Met. Phys.* **9** 1665
[42] Menshikov A Z 1989 *Physica* B **161** 1
[43] Endoh Y and Ishikawa Y 1971 *J. Phys. Soc. Japan* **30** 1614
[44] Acet M, Zähres H, Stamm W, Wassermann E F and Pepperhoff W 1989 *Physica* B **161** 67
[45] Schneider T, Acet M, Rellinghaus B, Wassermann E F and Pepperhoff W 1995 *Phys. Rev.* B **51** 8917